Supporting information for "A Numerical Model for Offshore Geological Carbon Storage (GCS) Undergoing Hydrate Formation"

Yufei Wang[1], Eric Flauraud[1], Anthony Michel[1],Veronique Lachet[2], Clementine Meiller[3]

[1]Dept. of Applied Mathematics. IFP Energies Nouvelles, 1 et 4 Avenue du Bois-Préau, 92825 Rueil-Malmaison, France
[2]Dept. of Thermo and Molecular Model. IFP Energies Nouvelles, 1 et 4 Avenue du Bois-Préau, 92825 Rueil-Malmaison, France
[3]Dept. of Computational Physics Porous Medium. IFP Energies Nouvelles, 1 et 4 Avenue du Bois-Préau, 92825 Rueil-Malmaison, France

Corresponding author: Yufei Wang, cnyufeiwang@gmail.com;yufei.wang@pku.edu.cn

Abstract

Here, we give the following supporting formation. First, we give the derivation of the energy balance equation for heat transfer in Section 1. Second, we give the derivation of the analytical solution for one-dimensional temperature distribution due to Joule-Thomson effect in Section 2. Third, we give the calculation of the density and viscosity of the CO_2-rich phase and brine in Section 3. Fourth, we give the information for the activity, the fugacity and the equilibrium constant for the chemical reaction module in Section 4. Fifth, we give the description of the kinetic rate law for hydrate formation and dissociation in Section 5. Sixth, we give sensitivity analysis on how the CO_2 hydration procedure is affected by the kinetic reaction rate, the brine salinity and the injection temperature in Section 6.

1 Derivation of the Energy Balance Equation

The motivation of offering the derivation for the energy balance equation is that some models for simulating non-isothermal multiphase flow with gas hydration do not properly calculate the thermal effect of hydrate formation/ dissociation [e.g. *Moridis*, 2012; *Gupta et al.*, 2015; *You and Flemings*, 2018; *Teng and Zhang*, 2020; *Yamaguchi et al.*, 2023], while some models make no difference between enthalpy and internal energy [e.g. *Sánchez et al.*, 2018].

In the following, we will offer the derivation on how to reach the energy balance equation employed in the model, i.e.,

$$0 = f_e = \frac{\partial}{\partial t}\left(\sum_{\alpha=l,g,HYD,Rock} \theta_\alpha \rho_\alpha \mathcal{U}_\alpha\right) + \nabla \cdot \left(\sum_{\alpha=l,g} \rho_\alpha \boldsymbol{q}_\alpha h_\alpha - \Lambda \nabla T\right) - Q^e, \tag{1}$$

where, θ_α [-] denotes the volumetric fraction of α phase with respect to the reference cell volume V_r [m^3]; ρ_α [$kg\cdot m^{-3}$] is the density of α phase; $\mathcal{U}_\alpha$ [$J\cdot kg^{-1}$] represents the specific internal energy of α phase; $\boldsymbol{q}_\alpha$ [$m\cdot s^{-1}$] represents the Darcy's discharge; h_α [$J\cdot kg^{-1}$] represents the specific enthalpy of α phase; Λ [$J\cdot m^{-1}\cdot s^{-1}\cdot K^{-1}$] is the heat conductivity; T [K] is the temperature; and Q^e [$J\cdot m^{-3}\cdot s^{-1}$] is the external source or sink of heat, which does not include the heat effect due to hydration. We note that we assume that the solid and fluid phases are in local thermal equilibrium.

Here, we start the derivation of (1) from the original energy conservation equation, which is given as [*Chen et al.*, 2006]

$$\begin{aligned} 0 = f_e = \frac{\partial}{\partial t}\left(\sum_{\alpha=l,g,HYD,Rock} \theta_\alpha \rho_\alpha \mathcal{U}_\alpha + \frac{1}{2}\sum_{\alpha=l,g} \rho_\alpha |\boldsymbol{q}_\alpha|^2\right) \\ + \nabla \cdot \left(\sum_{\alpha=l,g} \rho_\alpha \boldsymbol{q}_\alpha \left(\mathcal{U}_\alpha + \frac{1}{2}|\boldsymbol{q}_\alpha|^2\right) - \Lambda \nabla T\right) \\ + \sum_{\alpha=l,g} \left(\nabla \cdot (p_\alpha \boldsymbol{q}_\alpha) - \rho_\alpha \boldsymbol{q}_\alpha g \nabla z\right) - Q^e, \end{aligned} \tag{2}$$

where $\sum_{\alpha=l,g} \left(\nabla \cdot (p_\alpha \boldsymbol{q}_\alpha) - \rho_\alpha \boldsymbol{q}_\alpha g \nabla z\right)$ is the work due to pressure and gravity. Considering that for the fluid phases

$$\mathcal{U}_\alpha = h_\alpha - \frac{p_\alpha}{\rho_\alpha}, \tag{3}$$

equation (2) changes to

$$0 = f_e = \frac{\partial}{\partial t}\left(\sum_{\alpha=l,g,HYD,Rock} \theta_\alpha \rho_\alpha \mathcal{U}_\alpha + \frac{1}{2}\sum_{\alpha=l,g} \rho_\alpha |\boldsymbol{q}_\alpha|^2\right) + \nabla \cdot \left(\sum_{\alpha=l,g} \rho_\alpha \boldsymbol{q}_\alpha \left(h_\alpha + \frac{1}{2}|\boldsymbol{q}_\alpha|^2\right) - \Lambda \nabla T\right) - \sum_{\alpha=l,g} \rho_\alpha \boldsymbol{q}_\alpha g \nabla z - Q^e. \tag{4}$$

If we neglect the kinetic energy per unit bulk volume (i.e., terms including $|\boldsymbol{q}_\alpha|^2$) and the gravity potential energy term (i.e., $\sum_{\alpha=l,g} \rho_\alpha \boldsymbol{q}_\alpha g \nabla z$), equation (4) changes to the final equation (1).

If we only consider a static system without any source term, equation (1) becomes

$$0 = f_e = \frac{d}{dt}\left(\sum_{\alpha=l,g} \theta_\alpha \rho_\alpha \mathcal{U}_\alpha + \sum_{\alpha=\mathrm{HYD},Rock} \theta_\alpha \rho_\alpha \mathcal{U}_\alpha\right). \tag{5}$$

The specific internal energy ($\mathcal{U}_\alpha$) is given as

$$\mathcal{U}_\alpha = h_\alpha - \frac{p_\alpha}{\rho_\alpha}, \text{ if } \alpha = l, g, \tag{6}$$

and

$$\mathcal{U}_\alpha = h_\alpha, \text{ if } \alpha = HYD, Rock. \tag{7}$$

The specific enthalpy (h_α) is calculated as

$$h_\alpha(T) = h_{ref,\alpha} + c_\alpha(T - T_{ref}), \text{ for } \alpha = l, HYD, Rock, \tag{8}$$

and

$$h_\alpha(T, p_\alpha) = h_{ref,\alpha} + c_\alpha(T - T_{ref}) - c_\alpha \mu_{JT}(p_\alpha - p_{ref,\alpha}), \text{ for } \alpha = g, \tag{9}$$

where, $h_{ref,\alpha}$, T_{ref} and $p_{ref,\alpha}$ represent the reference enthalpy, the corresponding temperature and pressure, respectively; and c_α [J·kg^{-1}K^{-1}] represents the specific heat capacity; μ_{JT} [K·pa^{-1}] represents the Joule-Thomson coefficient.

Neglecting the effect of pressure on the specific enthalpy and specific energy, equation (5) changes to

$$0 = f_e = \frac{d}{dt}[\theta_l \rho_l (h_{l,ref} + c_l(T - T_{ref})) + \theta_g \rho_g (h_{g,ref} + c_g(T - T_{ref}) + \theta_{\mathrm{HYD}} \rho_{\mathrm{HYD}} (h_{\mathrm{HYD},ref} + c_{\mathrm{HYD}}(T - T_{ref}) + \theta_{Rock} \rho_{Rock} (h_{Rock,ref} + c_{Rock}(T - T_{ref}))], \tag{10}$$

i.e.,

$$\frac{d(T - T_{ref})}{dt}[(\mathcal{M}_l c_l + \mathcal{M}_g c_g + \mathcal{M}_{\mathrm{HYD}} c_{\mathrm{HYD}} + \mathcal{M}_{Rock} c_{Rock})] = -\frac{d}{dt}[\mathcal{M}_l h_{l,ref} + \mathcal{M}_g h_{g,ref} + \mathcal{M}_{\mathrm{HYD}} h_{\mathrm{HYD},ref} + \mathcal{M}_{Rock} h_{Rock,ref}] - (T - T_{ref}) \frac{d}{dt}[(\mathcal{M}_l c_l + \mathcal{M}_g c_g + \mathcal{M}_{\mathrm{HYD}} c_{\mathrm{HYD}} + \mathcal{M}_{Rock} c_{Rock})], \tag{11}$$

where $\mathcal{M}_\alpha = \theta_\alpha \rho_\alpha$ denotes the mass per volume.

Equation (11) indicates that for an adiabatic system the temperature will change if there exists reaction among HYD, water and gas. If we want to keep a constant temperature in a static system with chemical reaction, we need to add or remove energy at a rate of

$$\begin{aligned} Q_{\Delta H} = \frac{d}{dt}[\mathcal{M}_l h_{l,ref} + \mathcal{M}_g h_{g,ref} + \mathcal{M}_{\mathrm{HYD}} h_{\mathrm{HYD},ref}] \\ +(T - T_{ref})\frac{d}{dt}[\mathcal{M}_l c_l + \mathcal{M}_g c_g + \mathcal{M}_{\mathrm{HYD}} c_{\mathrm{HYD}} + \mathcal{M}_{Rock} c_{Rock}] \\ = r_k[-6 \cdot M_l h_{l,ref} - M_g h_{g,ref} + M_{\mathrm{HYD}} h_{\mathrm{HYD},ref}] \\ +r_k[-6 \cdot c_l M_l (T - T_{ref}) - c_g M_g (T - T_{ref}) + c_{\mathrm{HYD}} M_{\mathrm{HYD}} (T - T_{ref})], \end{aligned} \tag{12}$$

i.e., equation (10) for chemical reaction within a constant temperature system is

$$\begin{aligned} 0 = f_e = \frac{d}{dt}[\theta_l \rho_l (h_{l,ref} + c_l (T - T_{ref})) + \theta_g \rho_g (h_{g,ref} + c_g (T - T_{ref}) \\ +\theta_{\mathrm{HYD}} \rho_{\mathrm{HYD}} (h_{\mathrm{HYD},ref} + c_{\mathrm{HYD}} (T - T_{ref}) + \theta_{Rock} \rho_{Rock} (h_{Rock,ref} + c_{Rock} (T - T_{ref}))] - Q_{\Delta H}, \end{aligned} \tag{13}$$

where M_l, M_g and M_{HYD} represent the molecular weight of water, CO_2 and HYD, respectively.

Equation (13) can also be derived in another approach, given in the following.

For a system with constant temperature, the energy equation for each species is given as

$$0 = f_l = \frac{d}{dt}[\theta_l \rho_l (h_{l,ref} + c_l (T - T_{ref}))] + 6 r_k \cdot M_l (h_{l,ref} + c_l (T - T_{ref})) \tag{14}$$

$$0 = f_g = \frac{d}{dt}[\theta_g \rho_g (h_{g,ref} + c_g (T - T_{ref})] + r_k M_g (h_{g,ref} + c_g (T - T_{ref})) \tag{15}$$

$$0 = f_{\mathrm{HYD}} = \frac{d}{dt}[\theta_{\mathrm{HYD}} \rho_{\mathrm{HYD}} h_{\mathrm{HYD},ref} + c_{\mathrm{HYD}} (T - T_{ref})] - r_k M_{\mathrm{HYD}} (h_{\mathrm{HYD},ref} + c_{\mathrm{HYD}} (T - T_{ref})) \tag{16}$$

and

$$0 = f_{Rock} = \frac{d}{dt}[\theta_{Rock} \rho_{Rock} (h_{Rock,ref} + c_{Rock} (T - T_{ref}))]. \tag{17}$$

If we sum equations (14) to (17), we will get equation (13).

2 Analytical Solution for Heat Transfer in One-Dimensional Linear Domain

For a linear domain with only gas being the mobile phase (e.g., the water saturation is equal to or less than the residual saturation), we can get one analytical solution for the temperature development, provided that (1) the gas is incompressible, (2) the heat conduction is neglected and (3) the pressure distribution does not change with time. The governing equation for energy conservation in the above-mentioned system is given as follows

$$\phi S_{li} \rho_l \frac{\partial \mathcal{U}_l}{\partial t} + \phi (1 - S_{li}) \rho_g \frac{\partial \mathcal{U}_g}{\partial t} + (1 - \phi) \rho_r \frac{\partial \mathcal{U}_r}{\partial t} + \rho_g q_g \frac{\partial h_g}{\partial x} = 0, \tag{18}$$

where, $\phi (= \theta_l + \theta_g)$ is the total volume fraction of the fluid phases, S_{li} is the initial saturation of the liquid phase, ρ_l, ρ_g and ρ_r are respectively the liquid, gas and rock densities, $\mathcal{U}_l$, $\mathcal{U}_g$ and $\mathcal{U}_r$ are respectively the specific internal energies of the liquid, gas and rock phases, h_g is the specific enthalpy of gas, and q_g is the Darcian flux of the gas phase. The constitutional equations for the specific energies and enthalpies are given by equations (6) to (9). The Darcian discharge of gas phase is given as

$$q_g = -\kappa \frac{\kappa_{r,gi}}{\mu_g} \frac{\partial p_g}{\partial x}, \tag{19}$$

where $\kappa_{r,gi}$ is the relative permeability of gas phase that is a function of liquid saturation and thus does not change with time, and μ_g is the gas viscosity.

The initial condition is given as

$$T(x,0) = T_0,\ p_g(x,0) = p_{g,in} - \frac{x}{L}(p_{g,in} - p_{g,out}), \tag{20}$$

where T_0 denotes the initial temperature, and $p_{g,in}$ and $g_{g,out}$ respectively represent the gas pressure at the left inlet and right outlet boundaries. The boundary condition is given as

$$T(0,t) = T_{inj},\ p_g(0,t) = p_{g,in},\ p_g(L,t) = p_{g,out}, \tag{21}$$

where T_{inj} is the temperature of the gas flowing inside the domain through the left inlet boundary.

Considering that the pressures and the densities will not change in the process, equation (18) can be written in the form

$$\left[\phi S_{li}\rho_l c_l + \phi(1-S_{li})\rho_g c_g + (1-\phi)\rho_r c_r\right]\frac{\partial T}{\partial t} + \rho_g q_g c_g\left(\frac{\partial T}{\partial x} - \mu_{jt}\frac{\partial p_g}{\partial x}\right) = 0. \tag{22}$$

Defining the reference velocity constant

$$q_g^* = \frac{\rho_g q_g c_g}{\phi S_{li}\rho_l c_l + \phi(1-S_{li})\rho_g c_g + (1-\phi)\rho_r c_r}, \tag{23}$$

we can obtain

$$\frac{\partial T}{\partial t} + q_g^*\left(\frac{\partial T}{\partial x} - \mu_{jt}\frac{\partial p_g}{\partial x}\right) = 0. \tag{24}$$

Defining $T^* = T - \mu_{jt}p_g$, equation (24) can be written as

$$\frac{\partial T^*}{\partial t} + q_g^*\frac{\partial T^*}{\partial x} = 0. \tag{25}$$

The initial and boundary conditions now are rewritten as

$$T^*(x,0) = T_0 - \mu_{jt}p_g(x), \tag{26}$$

and

$$T^*(0,t) = T_{inj} - \mu_{jt}p_{g,in}. \tag{27}$$

The solution of equation (25) constrained by conditions (26) and (27) is going to be solved with characteristic method. The solution is given as

$$T^*(x,t) = \begin{cases} T^*(0,t),\ 0 < x < q_g^* t \\ T^*(x - q_g^* t, 0),\ q_g^* t < x < L. \end{cases} \tag{28}$$

that is

$$T(x,t) = \begin{cases} T_{inj} - \mu_{jt}\left[p_{g,in} - p_g(x)\right], 0 < x < q_g^* t \\ T_0 - \mu_{jt}\left[p_g(x - q_g^* t) - p_g(x)\right], q_g^* t < x < L. \end{cases} \tag{29}$$

3 Densities and Viscosities

Brine Density

We assume the brine density, ρ_l [kg$\cdot$ m^{-3}], depends on brine phase pressure, temperature, molality of Na^+ and Cl^-, and CO_2 concentration. The expression for brine is given as [*Garcia*, 2003]

$$\rho_l = \rho_{lr} + c \cdot M_{CO_2} - c \cdot \rho_{lr} \cdot V_\phi, \tag{30}$$

where, c [mol$\cdot$m^{-3}] is number of moles of aqueous CO_2 per unit volume of brine phase; M_{CO_2} [kg$\cdot$mol^{-1}] is the molecular weight of CO_2; V_ϕ [m$^3\cdot$ mol^{-1}], the apparent molar volume of CO_2, is given as

$$V_\phi = 3.751 \times 10^{-5} - 9.585 \times 10^{-8} T_c + 8.74 \times 10^{-10} T_c^2 - 5.044 \times 10^{-13} T_c^3, \tag{31}$$

where T_c [°C] is temperature in Celsius; ρ_{lr}, the brine density when there is no CO_2 dissolution, can be calculated with [*Phillips et al.*, 1982]

$$\rho_{lr} = -3.033405 \times 10^3 + 1.0128163 \times 10^4 \iota - 8.750567 \times 10^3 \iota^2 + 2.66310 \times 10^3 \iota^3, \tag{32}$$

with

$$\begin{aligned} \iota = &- 9.9595 \exp\left(-4.539 \times 10^{-3} m^S\right) + 7.0845 \exp\left(-1.638 \times 10^{-4} T_c\right) \\ &+ 3.9093 \exp\left(2.551 \times 10^{-10} p_l\right), \end{aligned} \tag{33}$$

where, m^S [molal] is mean molality of Na^+ anf Cl^- and p_l [pa] is the pressure of brine.

Rearranging Equation (30), we have [*Riano-Vilarrasa*, 2012]

$$\rho = \rho_{lr} \frac{1}{1 - X^C f_\delta} \approx \rho_{lr} (1 + X^C f_\delta), \tag{34}$$

with

$$f_\delta = 1 - \rho_{lr} \frac{V_\phi}{M_{CO_2}}; \tag{35}$$

here X^C denotes the mass fraction of aqueous CO_2.

CO_2 Density

The density of CO_2-rich phase is solved by first obtaining the molar volume of CO_2 phase (V [m$^3\cdot$mol^{-1}]) through solving the cubic form of Redlich-Kwong equation [*Redlich and Kwong*, 1949]:

$$V^3 - V^2 \left(\frac{\mathcal{R}T}{p_g}\right) - V \left(\frac{\mathcal{R}T \mathsf{b}^{CO_2}}{p_g} - \frac{\mathsf{a}^{CO_2}}{p_g T^{0.5}} + \left(\mathsf{b}^{CO_2}\right)^2\right) - \left(\frac{\mathsf{a}^{CO_2} \mathsf{b}^{CO_2}}{p_g T^{0.5}}\right) = 0, \tag{36}$$

where, a^{CO_2} [bar$\cdot$cm$^6\cdot$K$^{0.5}\cdot$mol^{-2}] and b^{CO_2} [cm$^3\cdot$mol^{-1}] are, respectively, the intermolecular attraction and repulsion of the CO_2-rich phase; $\mathcal{R} = 8.314$ [J$\cdot$K$^{-1}\cdot$ mol^{-1}] is the universal gas constant; T [K] is temperature in Kelvin; and p_g [bar] is gas pressure. According to *Spycher et al.* [2003], we have

$$\mathsf{a}^{CO_2} = 7.54 \times 10^7 - 4.13 \times 10^4 T, \tag{37}$$

and

$$\mathsf{b}^{CO_2} = 27.8. \tag{38}$$

Here, we note that Equation (36) may have more than one real solutions. The selection of the value depends on which phase- gas or liquid-is more stable. If the more stable phase is gas then we choose the maximum value (V_{max}); otherwise, we choose the minimum value (V_{min}). To determine which phase is more stable, we need to calculate two works (w_1 and w_2) for phase transition:

$$w_1 = p_g \left(V_{max} - V_{min}\right), \tag{39}$$

and

$$w_2 = \mathcal{R}T \ln \frac{V_{max} - \mathsf{b}^{\mathrm{CO_2}}}{V_{min} - \mathsf{b}^{\mathrm{CO_2}}} + \frac{\mathsf{a}^{\mathrm{CO_2}}}{T^{0.5}\mathsf{b}^{\mathrm{CO_2}}} \ln \frac{\left(V_{max} + \mathsf{b}^{\mathrm{CO_2}}\right) V_{min}}{\left(V_{min} + \mathsf{b}^{\mathrm{CO_2}}\right) V_{max}}. \tag{40}$$

If $w_2 \geq w_1$, then gaseous state is more stable and we choose V_{max}; otherwise, we choose V_{min}.

Finally, we obtain the density of CO_2 phase:

$$\rho_g = \frac{M_{\mathrm{CO_2}}}{V}. \tag{41}$$

Brine Viscosity

The viscosity of brine is calculated by [*Garcia*, 2003; *Kumagai and Yokoyama*, 1999]

$$\begin{aligned}\mu_l =& (3.85971 - 1.32561 \times 10^{-2}T)m^S + (-5.37539 + 1.90621 \times 10^{-2}T)(m^S)^{1/2} \\ &+ (8.79552 - 3.17229 \times 10^{-2}T)m^C + (-7.22796 + 2.64498 \times 10^{-2}T)(m^C)^2 \\ &+ 1.69956 \times 10^{-9}(p_l - 1 \times 10^5) + \mu_w(T, p = 10^5[\mathrm{Pa}]),\end{aligned} \tag{42}$$

where, T [K] is temperature in Kelvin, m^C [molal] is the molality of CO_2, and μ_w [mPa· s] is the viscosity of pure water.

CO_2 Viscosity

The viscosity of CO_2-rich phase(μ_g [μPa· s]) is assumed to be a function of temperature and pressures. The formula is given as [*Sovová and Procházka*, 1993; *Riano-Vilarrasa*, 2012]

$$\mu_g = \mu_0 \exp\left(\sum_{i=1}^{4}\sum_{j=0}^{1} \frac{a_{i,j}\rho_R^i}{T_R^j}\right), \tag{43}$$

where,

$$\mu_0 = T_R^{0.5}\left(27.2246461 - \frac{16.346068}{T_R} + \frac{4.66920556}{T_R^2}\right). \tag{44}$$

Here, scaled density $\rho_R = \rho_g/\rho_{cr}$ and scaled temperature $T_R = T/T_{cr}$; the critical density of CO_2 $\rho_{cr} = 468$ [kg·m^{-3}] and the critical temperature of CO_2 $T_{cr} = 304$ [K]; The coefficients: $a_{1,0} = 0.248566120$, $a_{1,1} = 0.004894942$, $a_{2,0} = -0.373300660$, $a_{2,1} = 1.22753488$, $a_{3,0} = 0.363854523$, $a_{3,1} = -0.774229021$, $a_{4,0} = -0.0639070755$ and $a_{4,1} = 0.142507049$. We note that the unit of viscosity obtained by Equation (43) is [μPa·s].

4 Activities, Fugacities and Equilibrium Constants

The activity of the solid phase is equal to unit. The activity of water species is equal to the molar fraction of water in the liquid phase, i.e.,

$$a_{\mathrm{H_2O}} = x_{\mathrm{H_2O}} = \frac{\xi_{\mathrm{H_2O}}/M_{\mathrm{H_2O}}}{\xi_{\mathrm{H_2O}}/M_{\mathrm{H_2O}} + \xi_{\mathrm{CO_2(aq)}}/M_{\mathrm{CO_2(aq)}} + \xi_{\mathrm{Na^+}}/M_{\mathrm{Na^+}} + \xi_{\mathrm{Cl^-}}/M_{\mathrm{Cl^-}}}, \tag{45}$$

where $x_{\mathrm{H_2O}}$ represents the molar fraction of water, M_i and ξ_i respectively denote the molecular weight and the mass of species i [*Spycher et al.*, 2003; *Spycher and Pruess*, 2005].

The activities of the ions ($a_{\mathrm{Na^+}}$ and $a_{\mathrm{Cl^-}}$) are simply equal to their molality, by assuming the activity coefficient is equal to one, i.e.,

$$a_{\mathrm{Na^+,Cl^-}} = m_{\mathrm{Na^+,Cl^-}}, \tag{46}$$

where $m_{\mathrm{Na^+}}$ and $m_{\mathrm{Cl^-}}$ represent the molality of Na^+ and Cl^-, respectively [*Saaltink et al.*, 1998].

The activity of aqueous CO_2 is calculated by

$$a_{CO_2} = \gamma_{CO_2} m_{CO_2}, \tag{47}$$

where the activity coefficient of aqueous CO_2 is given by [*Duan and Sun*, 2003]

$$\gamma_{CO_2} = 2\lambda_\gamma m_{Na^+} + \xi_\gamma m_{Cl^-} m_{Na^+}, \tag{48}$$

where

$$\begin{aligned}\lambda_\gamma = &- 0.411370585 + 6.07632013^{-4} T + \frac{97.5347708}{T} - \frac{0.0237622469\, p_l}{T} \times 10^{-5} \\ &+ \frac{0.0170656236\, p_l}{630 - T_k} \times 10^{-5} + 1.41335834 \times 10^{-5} T \ln\left(p_l \times 10^{-5}\right)\end{aligned} \tag{49}$$

and

$$\begin{aligned}\xi_\gamma = &3.36389723 \times 10^{-4} - 1.98298980 \times 10^{-5} T + \frac{2.12220830 \times 10^{-3}\, p_l}{T_k} \times 10^{-5} \\ &- \frac{5.24873303 \times 10^{-3}\, p_l}{630 - T} \times 10^{-5}.\end{aligned} \tag{50}$$

Here, p_l is the liquid pressure in Pa and T is the temperature in K.

The fugacity of gaseous CO_2 is calculated with

$$f_{CO_2} = F_{CO_2} p_g, \tag{51}$$

where p_g is the gas pressure, and F_{CO_2} is the fugacity coefficient. Here, we note that the unit of CO_2 fugacity is pa and bar for hydration and dissolution reaction, respectively. F_{CO_2} is calculated as [*Spycher et al.*, 2003],

$$\begin{aligned}\ln F_{CO_2} = &\ln \frac{V}{V - \mathsf{b}^{CO_2}} + \frac{\mathsf{b}^{CO_2}}{V - \mathsf{b}^{CO_2}} - \ln \frac{V + \mathsf{b}^{CO_2}}{V} \frac{2}{\mathcal{R} T^{1.5} \mathsf{b}^{CO_2}} \mathsf{a}^{CO_2} \\ &+ \frac{\mathsf{a}^{CO_2} \mathsf{b}^{CO_2}}{\mathcal{R} T^{1.5} \left(\mathsf{b}^{CO_2}\right)^2} \left(\ln \frac{V + \mathsf{b}^{CO_2}}{V} - \frac{\mathsf{b}^{CO_2}}{V + \mathsf{b}^{CO_2}}\right) - \ln \frac{p_g V}{\mathcal{R} T},\end{aligned} \tag{52}$$

where a^{CO_2} [bar·cm^6· K$^{0.5}$·mol^{-2}] and b^{CO_2} [cm^3·mol^{-1}] are, respectively, the intermolecular attraction and repulsion of the CO_2-rich phase, and $\mathcal{R} = 8.314$ [J·K^{-1}· mol^{-1}] is the universal gas constant,. a^{CO_2} and b^{CO_2} are defined by Equations (37) and (38). The molar volume of CO_2 phase, V [m^3·mol^{-1}], is obtained by solving the cubic form of Redlich-Kwong equation (36).

The equilibrium constant for CO_2 dissolution (K_{CO_2}) is calculated as

$$K^{CO_2} = K_0^{CO_2} \exp \frac{\left(p_g - p^0\right) \overline{V}_{CO_2}}{\mathcal{R} T_c}, \tag{53}$$

with

$$K_0^{CO_2} = 10^{a_K + b_K T_c + c_K T_c^2}, \tag{54}$$

where, T_c is the temperature in °C, $\overline{V}_{CO_2}$ [cm^3· mol^{-1}] denotes the mean molar volume of pure condensed CO_2 gas when pressure change from p^0 to p_g. Here, we assume $\overline{V}_{CO_2}$ is a constant of 32.6 [cm^3· mol^{-1}] [*Spycher et al.*, 2003]. The parameters for Equation (54) are $a_K = 1.189$, $b_K = 1.304 \times 10^{-2}$ and $c_K = -5.446 \times 10^{-5}$ [*Spycher et al.*, 2003]. The equilibrium constant for halite dissolution is $10^{1.582}$.

5 Kinetic Rate Law for Hydrate Formation/Dissociation

The hydrate association and dissociation share the same rate law

$$r_k = -k_0 A_r \Gamma_r \exp\left(-\frac{E_a}{\mathcal{R}T}\right)(f_h - f), \tag{55}$$

with

$$k_0 = \begin{cases} k_{0,\mathcal{F}}, & f > f_h, \\ k_{0,\mathcal{D}}, & f < f_h, \end{cases} \tag{56}$$

and

$$E_a = \begin{cases} E_{a,\mathcal{F}}, & f > f_h, \\ E_{a,\mathcal{D}}, & f < f_h, \end{cases} \tag{57}$$

here, k_0 [mol·m^{-2}·pa^{-1}·s^{-1}] is the intrinsic kinetic rate constant, A_r [m^2·m^{-3}] is the specific area, Γ_r [-] describes the fraction of the reactive surface, E_a [J·mol^{-1}] denotes the activation energy, $\mathcal{R}$ (=8.314 [J·K^{-1}· mol^{-1}]) is universal gas constant, T [K] is temperature in Kelvin, f and f_h, respectively, represent the fugacity of CO_2 in CO_2-rich phase and the critical fugacity for hydrate formation/ dissociation, $k_{0,\mathcal{F}}$ and $k_{0,\mathcal{D}}$, respectively, denote the intrinsic kinetic rate constants for hydrate formation and dissociation, and $E_{a,\mathcal{F}}$ and $E_{a,\mathcal{D}}$, respectively, denote the activation energies for hydrate formation and dissociation. We note that the kinetic rate constant and the activation energy can be different for hydrate formation and dissociation procedures. We also define $k = k_0 \exp\left(-E_a/(\mathcal{R}T)\right)$ as the kinetic rate constant. In the model, we usually set k as constant.

Here, the gas phase is pure phase and fugacity equals to the gas pressure, i.e., $f_h = p_h$, and $f = p_g$, with p_h and p_g, respectively, represent the critical hydration pressure and the pressure of CO_2-rich phase. A_r is calculated based on

$$A_r = \frac{\phi^{1.5}}{\sqrt{\kappa}}, \tag{58}$$

where ϕ [-] is the total volume fraction of the fluid phases and κ [m^2] is the intrinsic permeability. Γ_r is defined as

$$\Gamma_r = \begin{cases} \frac{\xi_{\mathrm{HYD}}}{m_{ref}}, \text{ when } f > f_h; \\ \frac{\xi_{\mathrm{CO_2(g)}}}{m_{ref}}, \text{ when } f < f_h, \xi_{\mathrm{CO_2(g)}} < \frac{1}{6}\frac{M_{\mathrm{CO_2(g)}}}{M_{\mathrm{H_2O}}}\xi_{\mathrm{H_2O}}; \\ \frac{\xi_{\mathrm{H_2O}}}{m_{ref}}, \text{ when } f < f_h, \xi_{\mathrm{CO_2(g)}} > \frac{1}{6}\frac{M_{\mathrm{CO_2(g)}}}{M_{\mathrm{H_2O}}}\xi_{\mathrm{H_2O}}; \end{cases} \tag{59}$$

where, ξ_{HYD}, $\xi_{\mathrm{CO_2(g)}}$ and $\xi_{\mathrm{H_2O}}$, respectively, represent the masses of HYD, CO_2(g) and H_2O species, and m_{ref} is the reference mass. Here the mass of the rock is used as the reference mass. Other totally different model for hydrate formation is also proposed [*Sánchez et al.*, 2018].

Finally, we test the reaction module under different conditions. The initial hydrate mass is 1.0 [kg], the water mass is 1.0 [kg], and the gas pressure is constant (i.e., the gas supply is sufficient). We test four temperatures, two gas pressures, two salinities and four kinetic reaction rates. Therefore, we have in total test 64 cases. The summary of the parameters is listed in Table 1, and the simulation results are listed in Figures 1 to 4. From Figure 2, for instance, we can see the result for k =1E-9 and k =1E-10 are quite close for the hydrate association process and the same for the hydrate dissociation process, this means that the implicit algorithm can converge even if the time step is much larger than the half time of the kinetic reaction, and that the reaction will reach equilibrium state at one single time step if the time step is much larger than the half time of the kinetic reaction. Detailed discussions about the results are not given here.

6 Sensitivity analysis of kinetic reaction rate, brine salinity and injection temperature

In the following sensitivity analysis, the adopted parameters are the same as the reference case given in the main text supported by this document, except for the parameters to be analyzed.

Table 1: Parameter settings for the test of reaction module.

Parameter	**Symbol**	**Units**	**Values**
Temperature	T	[K]	(263.15,273.15,293.15,303.15)
Gas pressure	p_g	[bar]	(20,200)
Salinity	m_{NaCl}	[molal]	(3E-5,3)
Kinetic reaction rate constant	k	[mol·m^{-2}·pa^{-1}·s^{-1}]	(1E-12,1E-11,1E-10,1E-9)
Volume fraction of both fluid phases	ϕ	[-]	0.3
Intrinsic permeability	κ	[m^2]	1e-13
Initial water mass	$\xi_{\mathrm{H_2O}}$	[kg]	1.0
Initial HYD mass	ξ_{HYD}	[kg]	1.0

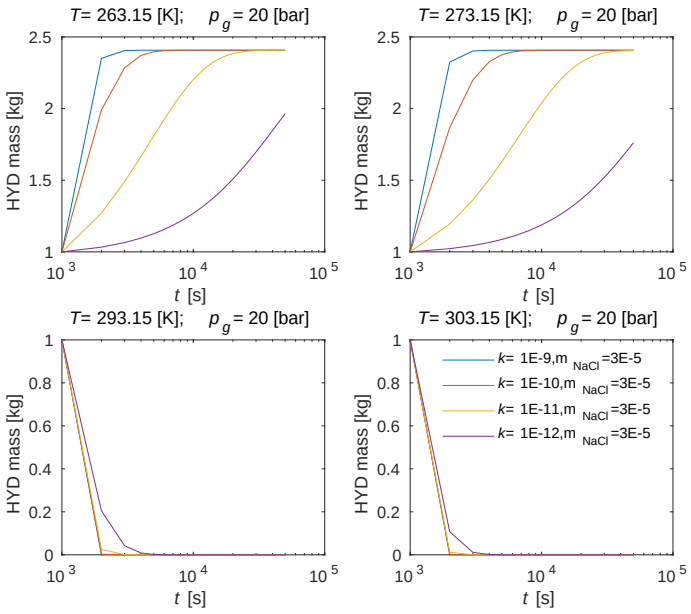

Figure 1: Hydration processes when the salinity m_{NaCl}=3E-5 [molal] and gas pressure p_g=20 [bar].

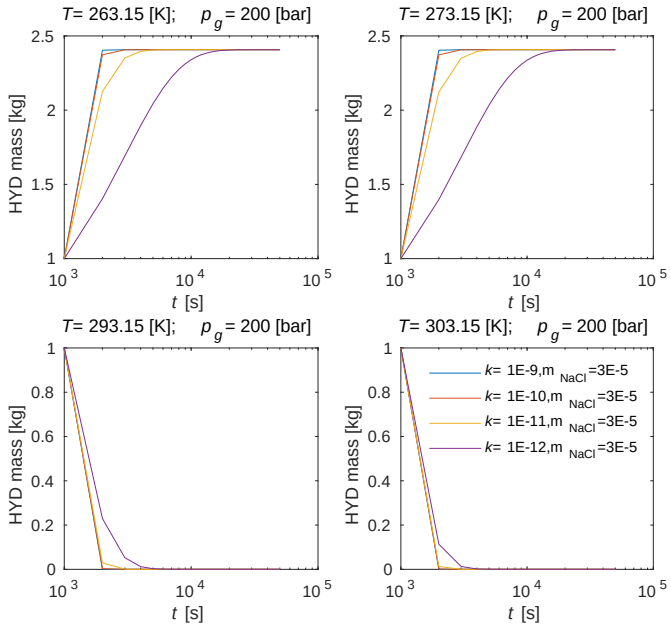

Figure 2: Hydration processes when the salinity m_{NaCl}=3E-5 [molal] and gas pressure p_g=200 [bar].

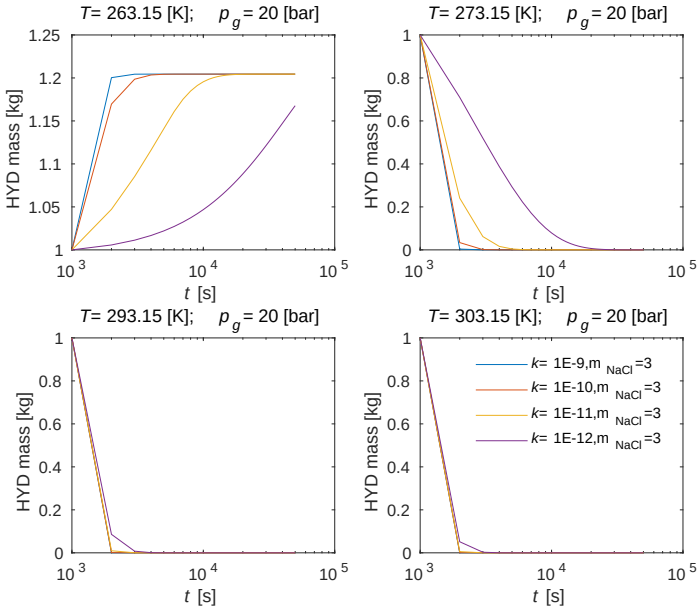

Figure 3: Hydration processes when the salinity m_{NaCl}=3.0 [molal] and gas pressure p_g=20 [bar].

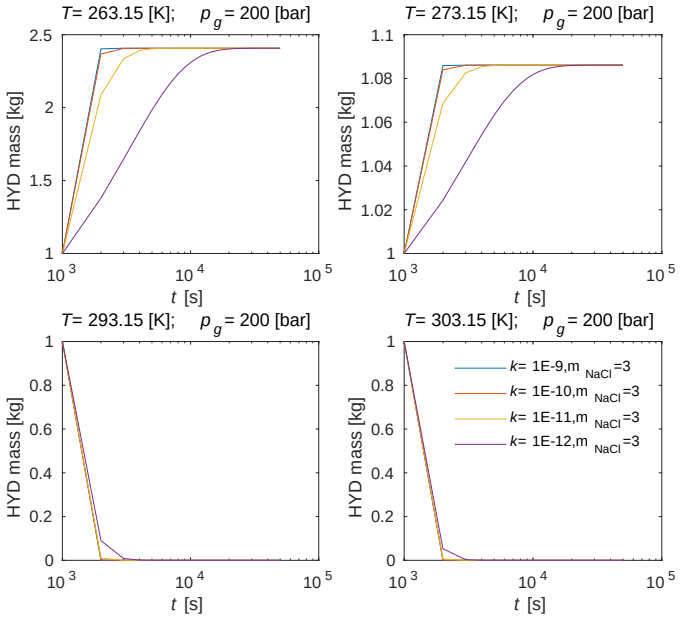

Figure 4: Hydration processes when the salinity m_{NaCl}=3.0 [molal] and gas pressure p_g=200 [bar].

First, we compare how the selection of the kinetic rate constant (k) affects the process by conducting additional three numerical simulations with different kinetic rate constants. Including the reference case, the kinetic rate constant ranges from 5.4×10^{-16} to 5.4×10^{-13} [mol·m^{-2}·pa^{-1}·s^{-1}]. The comparison of different reaction rates is shown in Figure 5, from which we can see that there is negligible difference between the results for $k = 5.4\times10^{-13}$ and $k = 5.4\times10^{-14}$, indicating that both of them can represent the equilibrium reaction in this setup. We note that the value of the reference kinetic rate constant ($k = 5.4\times10^{-13}$) is close to the reference value provided in literature [*Sun and Mohanty*, 2006; *Teng and Zhang*, 2020]. This means that in a reservoir scale simulation, the gas hydrate formation can be well treated as equilibrium reaction.

Second, the effect of salinity on hydration is analyzed by comparing the case with salinity $m_{\mathrm{NaCl}} = 2.0$ [molal] in contrast to the reference case of $m_{\mathrm{NaCl}} = 5 \times 10^{-5}$ [molal]. The comparison of the hydration procedure in reseroirs of different salinities is shown in Figure 6, from which we can see that for the case of high brine salinity, (1) the equilibrium temperature is lower than the injection temperature and hydrate cannot form in the vicinity of the injection point, (2) hydrate can form at a distance around 150 meters away from the injection point because of the temperature reduction due to the Joule-Thomson effect, and (3) the hydration driven by the Joule-Thomson effect is slow.

Finally, we analyze the effect of the injection temperature by comparing the reference case of injection temperature $T = 278.15$ [K] and the case of injection temperature $T = 293.15$ [K]. The comparison of the effect of the injection temperature on the hydrate formation is shown in Figure 7, from which we can see that for the case of injection temperature $T = 293.15$ [K], (1) the hydrate will not form in the vicinity of the injection point (i.e., $x = 0$) because the injection temperature is higher than the equilibrium temperature (around 283 [K]), (2) hydrate forms from $x \in (160, 320)$ [m] because the Joule-Thomson effect can reduce the temperature to a value below the critical hydration temperature, (3) the hydrate formation due to Joule-Thomson effect has small rate, and (4) the temperature in the hydrate formation zone is still equal to the equilibrium temperature.

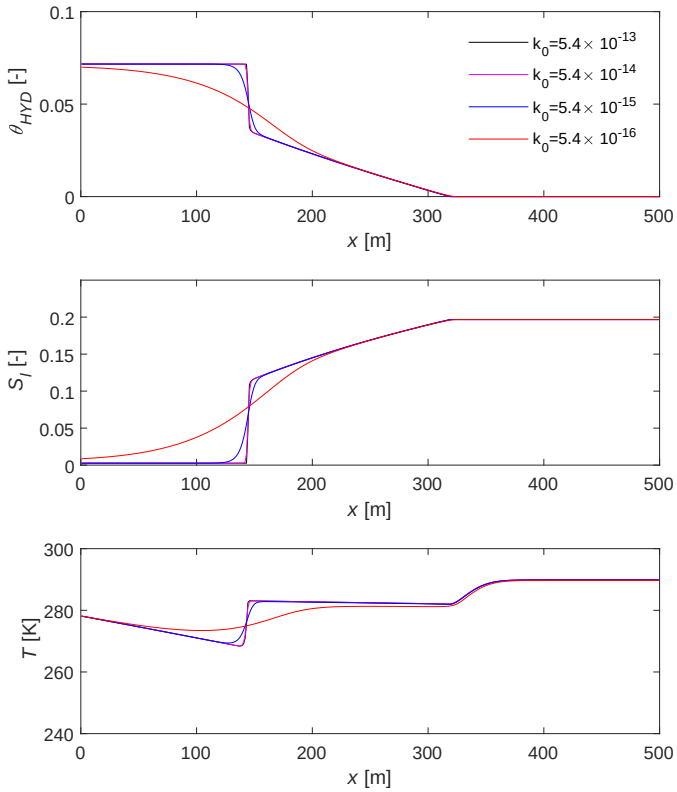

Figure 5: Comparison of hydrate formation under different kinetic rate constants.

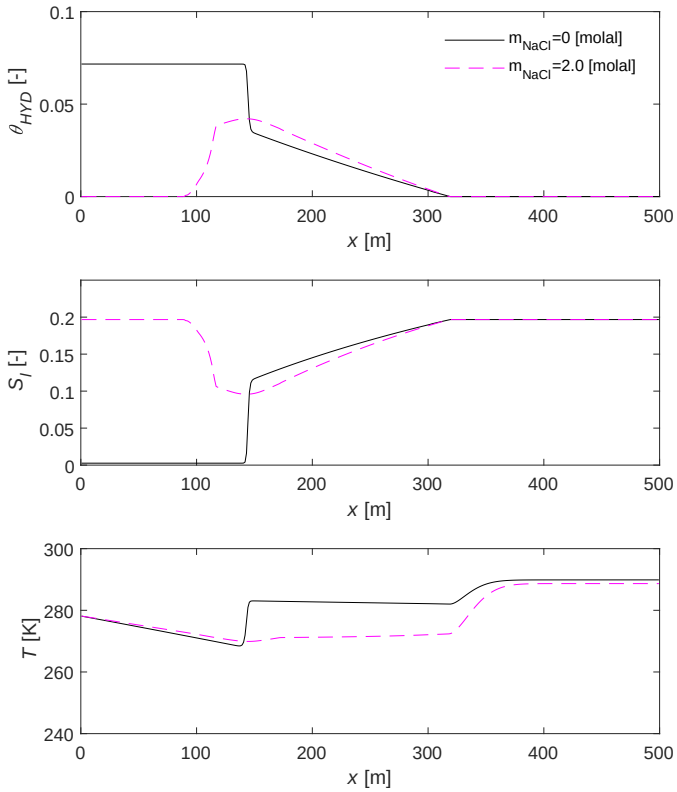

Figure 6: Comparison of hydrate formation in reservoirs of different salinities.

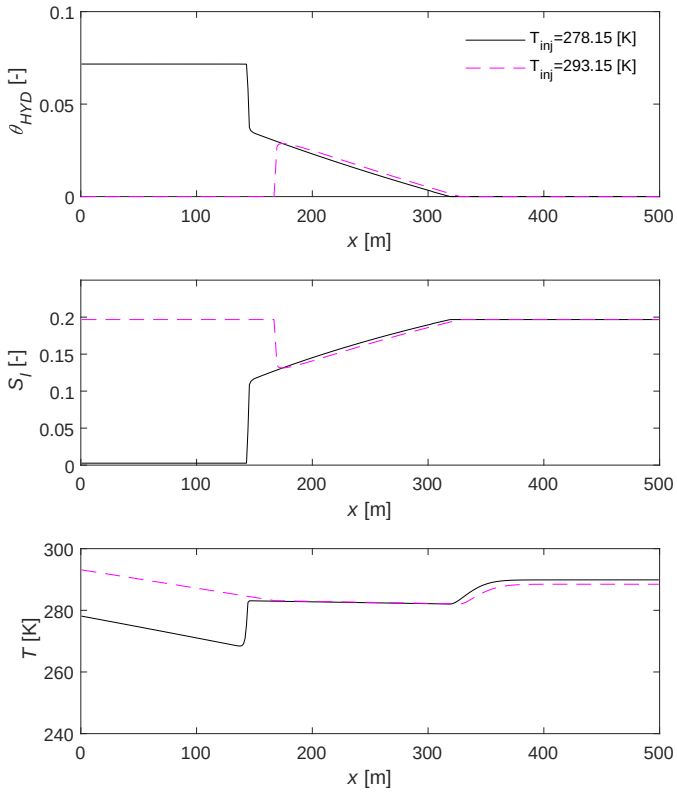

Figure 7: Comparison of the hydrate formation under different injection temperatures.

References

Chen, Z., G. Huan, and Y. Ma (2006), *Computational Methods for Multiphase Flows in Porous Media*, doi:10.1137/1.9780898718942.

Duan, Z., and R. Sun (2003), An improved model calculating CO 2 solubility in pure water and aqueous NaCl solutions from 273 to 533 K and from 0 to 2000 bar, *Chemical Geology*, doi:10.1016/S0009-2541(02)00263-2.

Garcia, J. E. (2003), Fluid Dynamics of Carbon Dioxide Disposal into Saline Aquifers, *TH: Thesis (Ph.D.); Submitted to the University of California, Berkeley, CA (US); PBD: 18 Dec 2003*.

Gupta, S., R. Helmig, and B. Wohlmuth (2015), Non-isothermal, multi-phase, multi-component flows through deformable methane hydrate reservoirs, *Computational Geosciences*, *19*, 1063–1088.

Kumagai, A., and C. Yokoyama (1999), Viscosities of aqueous NaCl solutions containing CO2 at high pressures, *Journal of Chemical and Engineering Data*, doi:10.1021/je980178p.

Moridis, G. J. (2012), Tough+ hydrate v1. 2 user's manual: A code for the simulation of system behavior in hydrate-bearing geologic media.

Phillips, S. L., A. Igbene, J. A. Fair, H. Ozbek, and M. Tavana (1982), Technical Databook for Geothermal energy utilization., in *Proceedings of the Symposium on Thermophysical Properties*.

Redlich, O., and J. N. Kwong (1949), On the thermodynamics of solutions. V. An equation of state. Fugacities of gaseous solutions, *Chemical Reviews*, doi:10.1021/cr60137a013.

Riano-Vilarrasa, V. (2012), Thermo-hydro-mechanical impacts of carbon dioxide (co2) injection in deep saline aquifers, Ph.D. thesis, Technical University of Catalonia.

Saaltink, M. W., C. Ayora, and J. Carrera (1998), A mathematical formulation for reactive transport that eliminates mineral concentrations, *Water Resources Research*, doi:10.1029/98WR00552.

Sánchez, M., C. Santamarina, M. Teymouri, and X. Gai (2018), Coupled numerical modeling of gas hydrate-bearing sediments: From laboratory to field-scale analyses, *Journal of Geophysical Research: Solid Earth*, *123*(12), 10–326.

Sovová, H., and J. Procházka (1993), Calculations of Compressed Carbon Dioxide Viscosities, *Industrial and Engineering Chemistry Research*, doi:10.1021/ie00024a029.

Spycher, N., and K. Pruess (2005), CO2-H2O mixtures in the geological sequestration of CO2. II. Partitioning in chloride brines at 12-100°C and up to 600 bar, *Geochimica et Cosmochimica Acta*, doi:10.1016/j.gca.2005.01.015.

Spycher, N., K. Pruess, and J. Ennis-King (2003), CO2-H2O mixtures in the geological sequestration of CO2. I. Assessment and calculation of mutual solubilities from 12 to 100°C and up to 600 bar, *Geochimica et Cosmochimica Acta*, doi:10.1016/S0016-7037(03)00273-4.

Sun, X., and K. K. Mohanty (2006), Kinetic simulation of methane hydrate formation and dissociation in porous media, *Chemical Engineering Science*, *61*(11), 3476–3495.

Teng, Y., and D. Zhang (2020), Comprehensive study and comparison of equilibrium and kinetic models in simulation of hydrate reaction in porous media, *Journal of Computational Physics*, *404*, 109,094.

Yamaguchi, A. J., T. Sato, T. Tobase, X. Wei, L. Huang, J. Zhang, J. Bian, and T.-Y. Liu (2023), Multiscale numerical simulation of co2 hydrate storage using machine learning, *Fuel*, *334*, 126,678.

You, K., and P. B. Flemings (2018), Methane hydrate formation in thick sandstones by free gas flow, *Journal of Geophysical Research: Solid Earth*, *123*(6), 4582–4600.